machines

MDPI

Article

Comparative Analysis of Current and Voltage THD at Different Grid Powers for Powerful Active Front-End Rectifiers with Preprogrammed PWM

Alexander S. Maklakov [1,*], Tao Jing [2] and Alexander A. Nikolaev [3]

[1] Project Activity Center, Scientific Activity Sector, Moscow Polytechnic University, 107023 Moscow, Russia
[2] School of Mechanical and Electrical Engineering, China Jiliang University, Hangzhou 310018, China
[3] Department of Automated Electric Drives and Mechatronics, Nosov Magnitogorsk State Technical University, 455000 Magnitogorsk, Russia
* Correspondence: alexandr.maklakov.ru@ieee.org

Abstract: Preprogrammed pulse width modulation (PPWM) techniques are drawing a great deal of interest due to their strong harmonic performance. However, there have not yet been any systematic studies or elaboration of the influence of different grid powers on current and voltage THD using PPWM. Therefore, this article focuses on a comparative analysis of current and voltage THD in a system with a three-phase, three-level active front-end (AFE) at different grid powers by applying PPWM. A six-pulse electric drive power circuit and one laboratory measurement platform were designed and set up to achieve the above goals. The comparative results were calculated up to the 50th (THD_{50}) and 100th (THD_{100}) harmonics against the frequency of the PPWM, ranging between 150 Hz and 750 Hz. The grid power and AFE power ratio was between 30 and 230 under three different AFE-consumed currents. The experimental results were analyzed and compared, and they demonstrated for the first time how the grid power and AFE power ratio with different PPWM patterns can influence current and voltage THD. The research results suggest that it is necessary to review the existing calculation methods for current and voltage THD using modern electric power quality standards. The results presented in this article also provide a reference point for researchers and engineers when considering the electromagnetic compatibility (EMC) of nonlinear consumers in the design of similar circuits.

Keywords: preprogrammed pulse width modulation; three-level active front-end rectifier; selective harmonic elimination; selective harmonic mitigation; total harmonic distortion

Citation: Maklakov, A.S.; Jing, T.; Nikolaev, A.A. Comparative Analysis of Current and Voltage THD at Different Grid Powers for Powerful Active Front-End Rectifiers with Preprogrammed PWM. *Machines* **2022**, *10*, 1139. https://doi.org/10.3390/machines10121139

Academic Editor: Alejandro Gómez Yepes

Received: 28 October 2022
Accepted: 26 November 2022
Published: 1 December 2022

1. Introduction

The use of power conversion systems based on active front-ends (AFEs) to regenerate power is one of the most efficient power-saving solutions for electric drives and distributed generation systems. Many researchers and engineers around the world are working to improve these systems. The main reasons for the widespread application of AFEs include high efficiency (95–98%), two-way electric power flow control with a set cos (φ), and compliance with international electromagnetic compatibility standards [1–4].

The limiting current and voltage values of semiconductor power systems allow for the use of two-level AFEs in low- and medium-power applications, usually up to 1 MW. As converted power increases, it is necessary to find new engineering solutions; the development of multilevel converter topologies is the most efficient. Currently, multilevel AFEs help ensure the electromagnetic compatibility of high-power consumers, ranging from tens to hundreds of megawatts. Neutral-point-clamped (NPC) is the most efficient and widely used multilevel topology. It is commonly limited to three levels, so academic publications often refer to NPC converters as three-level converters [5–7].

One reason for power quality problems in internal grids can be powerful electric drives with NPC AFE rectifiers. Studies have shown that these occur in cases of low grid power with long cable lines. Consequently, grid current resonance leads to high voltage harmonics at the point of common connection (PCC) of electrical consumers. The authors assessed the power quality in the grid of one metallurgical enterprise at the PCC with a 12 MW AFE electric drive of a rolling stand. A simplified power circuit of the electric drive is illustrated in Figure 1. The main characteristics of the circuit are presented in Table 1.

Table 1. Key parameters of the electric drive power circuit.

AFE Drive Power P, kW	Grid Power S_g, kVA	Connection	PWM Frequency, Hz
12,000	130,000	6-pulse, Y/Y	250

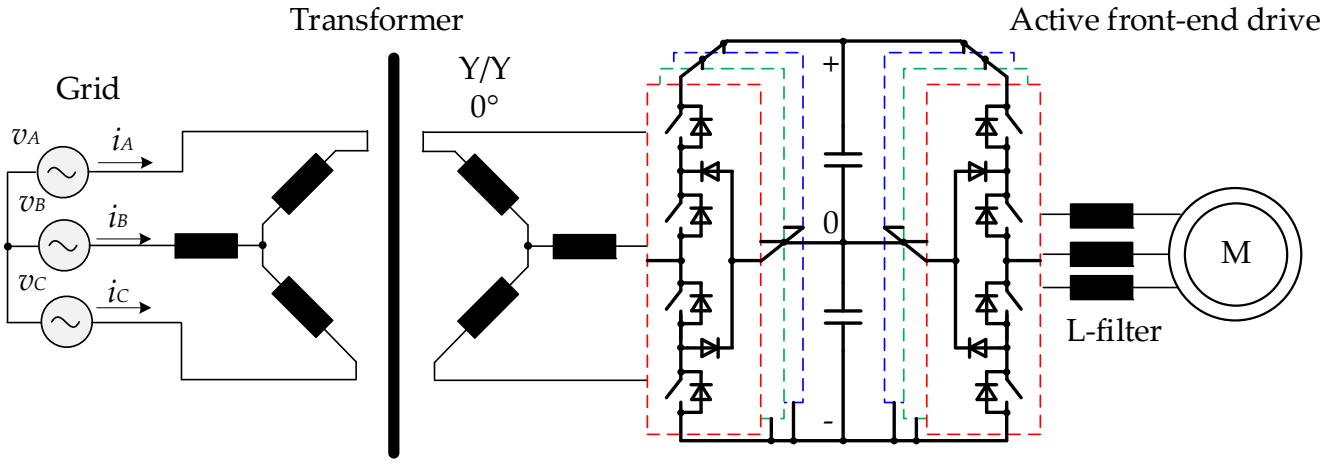

Figure 1. Six-pulse electric drive power circuit connection.

The experimental results were obtained by recording and subsequently analyzing the instantaneous values and spectrum of grid phase-to-phase voltages (U_{grid}). A measuring complex was used based on an ELSPEC G4420 power quality analyzer capable of long-term multichannel recording of the U_{grid} with a sampling frequency of 100 kHz. A photograph of the measuring complex is shown in Figure 2. The results presented in Figure 3a show that when the electric drive is switched off from the PCC, the U_{grid} does not contain significant high-order harmonics, and the THD is approximately 1%. The experiment proves that the main harmonic source in the power grid is the AFE electric drive of the rolling stand, since when it was connected, the voltage quality deteriorated significantly, as shown in Figure 3b. The harmonics with maximum voltage magnitudes (Mag, %) are numbered n = 23, 107, 109, and 113.

The efficiency of operation and the quality of the converted power of semiconductor converters largely depend on the selection of a specific pulse width modulation (PWM) strategy. The existing preprogrammed PWM (PPWM) method, based on the use of preprogrammed switching patterns for the semiconductor modules of converters, was designed to minimize the losses and increase the quality of the converted power. Researching, developing, and improving PPWM strategies is especially relevant for designing and ensuring the electromagnetic compatibility of three-level AFEs [8–10].

This study demonstrates, for the first time, how the ratio of the grid power and the AFEs at various patterns of PPWM with SHE can influence current and voltage THD. This article may shed light on the occurrence of electromagnetic compatibility problems in AFEs when the power system has insufficient power. The article is organized as follows: the Introduction describes the subject, explains the relevance of the study, and formulates its goals and objectives; Section 2 describes PPWM algorithms; Section 3 describes the

experimental facilities; Section 4 analyzes the modeling results; and Section 5 gives the conclusion.

Figure 2. Measuring complex.

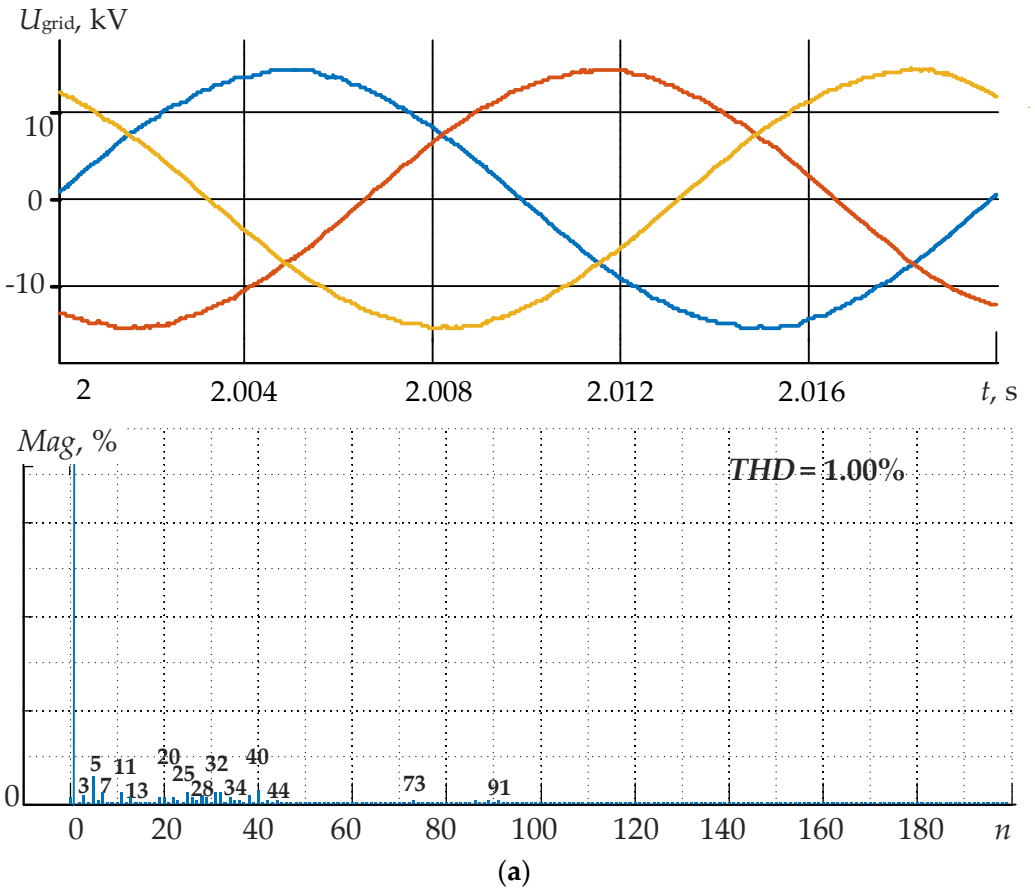

Figure 3. *Cont.*

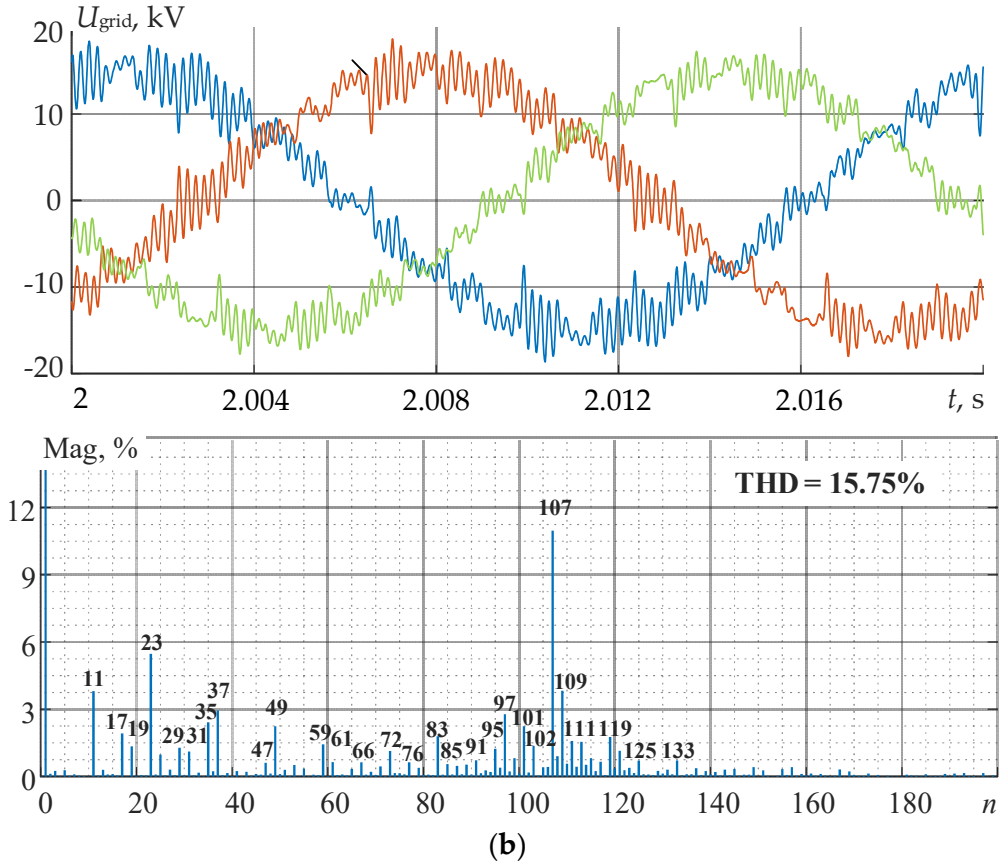

Figure 3. Results of experimental studies confirming the electromagnetic compatibility problems of powerful electric drives at insufficient grid power: (**a**) the AFE drive is switched off; (**b**) the AFE drive is switched on.

2. PPWM

2.1. Overview

Since the 1990s, there have been several trends in the development of the PPWM method that aim to resolve the research and engineering issues related to electromagnetic compatibility, energy efficiency, and increasing the power output of AFEs based on multi-level converter topologies [11–13]. When PPWM appeared, it attracted a lot of attention from experts in power conversion equipment all around the world. This method was also adapted to numerous application areas, mainly for high-voltage and high-power AFEs, where ensuring electromagnetic compatibility and switching losses are significant problems, and their resolution is a priority. PPWM demonstrates the following advantages [14–16]:

(1) Increased efficiency and quality parameters of the converted voltage;
(2) Increased effective converter voltage value;
(3) Reduced requirements for the filtering of feedback signals for converter currents and voltages;
(4) The opportunity to bypass the current and voltage resonance region without additional filter-compensating equipment;
(5) The opportunity to leave the harmonics that are divisible by three in the three-phase converter voltage system uncontrolled;
(6) The opportunity to control the levels of specific harmonic components and the total index of harmonic distortions of voltage/current.

The mathematical expression of the modulated converter voltage signal function u (ωt) for PPWM is based on Fourier-series decomposition and calculation of switching angles α

that help eliminate/control selected low-order harmonics. The general-case expression for $u(\omega t)$ can be written as follows:

$$u(\omega t) = \frac{a_0}{2} + \sum_{n=1}^{\infty} (a_n \cos(n\omega t) + b_n \sin(n\omega t)) \quad (1)$$

where ω is the angular frequency, n is the number of harmonics, and a_0, a_n, and b_n are the Fourier-series coefficients:

$$\begin{array}{l} a_0 = \frac{1}{\pi}\int_0^{2\pi} u(\omega t) \cdot d(\omega t), \\ a_n = \frac{1}{\pi}\int_0^{2\pi} u(\omega t) \cdot \cos(n\omega t) \cdot d(\omega t), \\ b_n = \frac{1}{\pi}\int_0^{2\pi} u(\omega t) \cdot \sin(n\omega t) \cdot d(\omega t). \end{array} \quad (2)$$

The most widespread waveform of converter voltage features quarter-wave symmetry. This form significantly simplifies Equation (1) [17]. Constant a_0 represents even harmonics, and sinusoidal coefficients of fuzzy harmonics equal zero, which transforms Equation (1) for a three-level signal waveform as follows:

$$u(\omega t) = \sum_{n=1,3,5,\ldots}^{\infty} \left(\frac{4}{n\pi} \left[\sum_{k=1}^{N} (-1)^{k+1} \cos(n\alpha_k) \right] \cdot \sin(n\omega t) \right) \quad (3)$$

where N is the number of switchings, and k is the sequence number of the switching angle from 1 to N.

The typical waveform of a three-level signal with quarter-wave symmetry is shown in Figure 4. The switching angles within the quarter period should keep the following ratios:

$$0 < \alpha_1 < \alpha_2 < \ldots < \alpha_N < \pi/2 \quad (4)$$

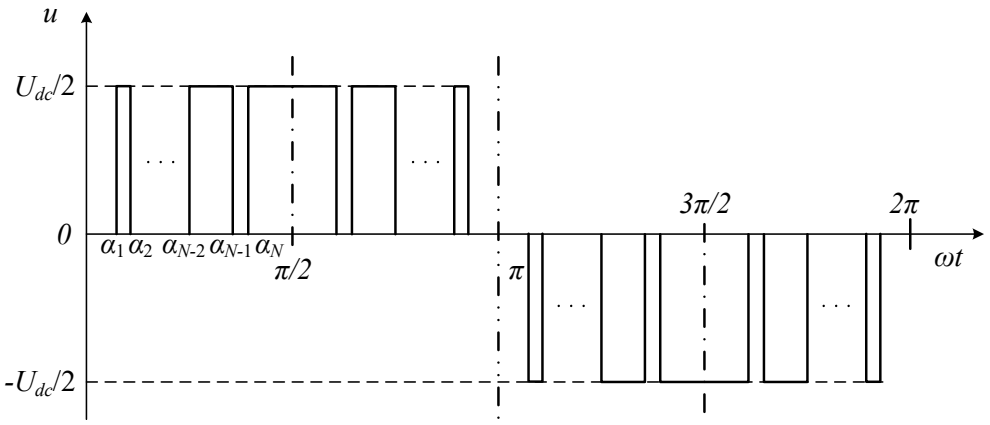

Figure 4. Waveform of a three-level signal with quarter-wave symmetry.

Academic publications suggest several approaches to signal spectrum formation using PPWM. All are based on searching for switching angles α using a specific optimality criterion. These may be classified as follows:

(1) Selective harmonic elimination (SHE);
(2) Selective harmonic mitigation (SHM).

2.2. Selective Harmonic Elimination

SHE is the most widespread approach to implementing the PPWM algorithm. It was first demonstrated in 1973 for a two-level AFE to eliminate some low-order harmonics in the AFE voltage spectrum. The implementation of this approach can be exemplified by the voltage waveform of a three-level converter with quarter-wave symmetry, as shown

in Figure 4 [18]. This waveform is set by the switching pattern of the AFE semiconductor modules at predetermined moments using the precalculated switching angles $\alpha_1, \alpha_2, \ldots, \alpha_N$, numbered N, over a quarter AFE voltage period that ranges between 0 and $\pi/2$, provided that $0 < \alpha_1 < \alpha_2 < \ldots < \alpha_N < \pi/2$.

The maximum number of switching angles N may be determined as follows:

$$N = \frac{f_{swave}}{f} \tag{5}$$

where f_{swave} is the average switching frequency for the AFE semiconductor modules, and f is the AFE voltage frequency.

Due to the quarter-wave symmetry of the signal waveform, only odd sinusoid components b_n are left after Fourier transformation:

$$\begin{cases} a_n = 0 \\ b_n = \begin{cases} 0, \\ \frac{4}{n\pi}\frac{U_{dc}}{2}\sum\limits_{k=1}^{N}(-1)^{k+1}\cos(n\alpha_k), \end{cases} \end{cases} \tag{6}$$

where U_{dc} is the AFE DC link voltage.

The number of harmonic components that can be equaled to zero in System (6) is limited by the number of semiconductor module switching occurrences and can be calculated using the following formula:

$$q = N - 1 \tag{7}$$

System (6) determines the correlation between the switching angles and the harmonic spectrum of an AFE signal as follows:

$$\begin{cases} U_1 = \sum\limits_{k=1}^{N}(-1)^{k+1}\cdot\cos(\alpha_k) = \frac{\pi}{4}\cdot M \\ U_n = \frac{4}{\pi}\cdot\sum\limits_{k=1}^{N}(-1)^{k+1}\cdot\cos(n\cdot\alpha_k) = 0, \ \textit{where } n = 5,\ 7,\ 11, \ldots \ . \end{cases} \tag{8}$$

where U_1 is the level of the fundamental harmonic, U_n is the level of harmonic n, and M is the modulation index between zero and $\frac{4}{\pi}$.

The set of solutions for the system of Equation (8) can be obtained as sequences of switching angles $\alpha_1, \alpha_2, \ldots, \alpha_N$ in the constraint region $0 < \alpha_1 < \alpha_2 < \ldots < \alpha_N < \pi/2$. Then, the most desirable solutions of each one are selected.

2.3. Selective Harmonic Mitigation

SHM was first used in 2007 for a three-level 150 kVA converter. This approach was based on satisfying voltage quality standards, particularly the total harmonic component (THD) coefficient and the levels of specific harmonic components of AFE voltage [19–22]. The equation defining the correlation between the switching angles and harmonic spectrum of the signal is as follows:

$$\begin{cases} \left|\frac{\pi}{4}\cdot M - U_1\right| \le L_1 \\ \frac{1}{|U_1|}\cdot\frac{4}{n\cdot\pi}\cdot\sum\limits_{k=1}^{N}(-1)^{k+1}\cdot\cos(n\cdot\alpha_k) \le L_n, \ \textit{where } n = 5,\ 7,\ 11,\ \ldots\ ,\ 49. \end{cases} \tag{9}$$

where L_1 is the constraint determining the level of the first harmonic, depending on the modulation coefficient, and L_n is the level constraint for every harmonic component n.

The sets of switching angles $\alpha_1, \alpha_2, \ldots, \alpha_N$ are in the constraint region $0 < \alpha_1 < \alpha_2 < \ldots < \alpha_N < \pi/2$. SHM allows for the identification of the switching angle sequence for the AFE semiconductor modules within the set constraints L_n corresponding to electric power quality standards.

The system of nonlinear equations describing the waveform of PPWM with SHE components can be solved using an array of mathematical methods. Current research concerning PPWM techniques is focused on mathematical algorithms to find new patterns [23–33]. During this research, the authors tested several of them, but the best results were produced using built-in functions of MATLAB software, namely *fsolve* and *fmincon*. Some PWM sequences were calculated and notated with the following codes: SHE3, SHE5, SHE7, SHE9, SHE11, SHE13, SHE15, SHM13, and SHM15.

3. Experiments

The research was carried out in a power conversion equipment laboratory. A generalized diagram of the test bench's hardware and software setup is shown in Figure 5. The specifications of the laboratory prototype and the testing system are presented in Table 2.

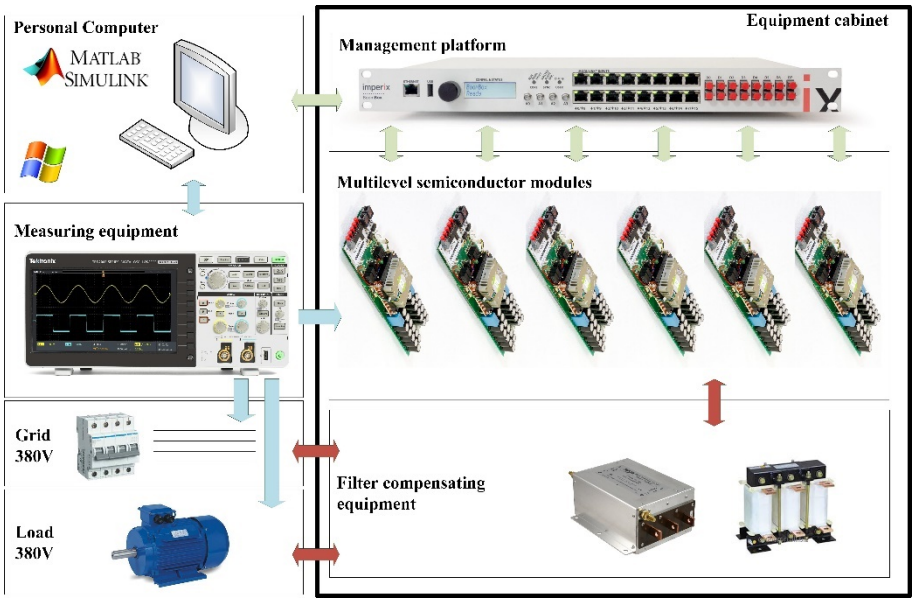

Figure 5. Main laboratory equipment.

Table 2. Main equipment specifications.

Power modules	1 × P924F33 Vincotech; reverse voltage IGBT, 600 V; permissible continuous current IGBT, 30 A; admissible continuous current of the reverse diode, 27 A; maximum switching frequency IGBT, 50 kHz; voltage drop, 1.5–2 V
Capacitors	2 × 517 µF Panasonic EEU-EE2W470S (two batteries of 11 × 47 µF each), maximum voltage, 450 V
Control drivers	4 × Avago ACPL-P345
Current sensor	1 × LEM HLSR 20-P/SP33, nominal range ± 20 A, 450 kHz; instrument error ± 1%
Voltage sensor	1 × resistive voltage divider + Avago ACPL-C87B, bandwidth, 25 kHz; instrument error ± 0.1%
FPGA	1 × Xilinx XC9536XL-10VQG44C, 10 ns; 36 microelements
Microcontrollers	2 × Microchip PIC24F04KA201, 16 bit, 16 MHz; 9 × 10-bit ADC; sampling rate, 500 ksps

Direct access to the control signal of the semiconductor modules was gained through optic-fiber inputs. Then, the galvanically isolated voltage probes of the DC and AC links at the converter input were connected to analog outputs. Overvoltage, overcurrent, and overheating protection were built into each converter's NPC cells, and the converters

were programmed by the researchers using a built-in microcontroller and a complex programmable logic device (CPLD). The mezzanine module was designed to transmit signals from optic inputs and analog outputs between the CPLD and the BoomBox control platform, including the digital signal processor (DSP) and the field programmable gate array (FPGA). The converter control tasks were distributed between the DSP and the FPGA. The FPGA controlled the correct distribution of the IGBT control impulses, and the DSP processed the converter control system program. The computing core of the DSP was a 32-bit TMS320C28346 processor manufactured by Texas Instruments with a clock rate of 300 MHz and featuring 256 MB NOR flash memory, 2 MB RAM, and 300 MIPS (with a floating point). The program code for the control platform was developed in MATLAB/Simulink. To take an oscillogram and measure the instant voltage values at the three-level converter input, we used the Windows^{TM}-based graphic software of the BoomBox control platform. We measured voltage signals using ModuLink isolated voltage probes for the range of $\pm$ 800 V with a bandpass of 60 kHz and a response of 2.46 mV/V. The probes were connected to the BoomBox control platform using the plug-and-play method and powered directly from the control platform. The output signal was transmitted over a screened twisted pair of probes integrated into RJ45 cables. Additional verification of the obtained oscillograms was carried out using a Tektronix TBS2072 oscilloscope with a bandpass of 80 MHz and a sampling frequency of 1 GSa/s, in addition to a differential HVP-08 sampler model.

Most AFE control systems are based on so-called voltage-oriented control (VOC). Linear controllers are either proportional (P) or proportional–integral (PI). Figure 6 depicts the circuit diagram of the AFE closed-loop control system used in the objective analysis. One special feature of this circuit is that the three-phase current signals i_{abc} and the three-phase voltage signals u_{abc} are measured at the primary side of the phase-shift transformer (T). This is possible since there are no other power-consuming devices. Figure 6 uses the following notation: T is the phase-shift transformer; PLL is the unit that synchronizes voltages with the secondary windings of the phase-shift transformer; i_{abc} and u_{abc} are the measured instantaneous phase currents and values on the primary side of the phase-shift transformer in the *abc* coordinates; θ is the grid voltage space vector angle for the secondary windings of the phase-shift transformer; i_{dq} is the measured instantaneous phase currents and values on the primary side of the phase-shift transformer in the *dq0* coordinates; i_{dqref} is the configured phase current of the AFE in the *dq0* coordinates; u_{dq} is the measured instantaneous phase voltage of the AFE in the *dq0* coordinates; u_{dc} is the measured instantaneous voltage of the DC link capacitors in the AFE; u_{dcref} is the configured AFE DC link capacitor voltages; M is the AFE modulation index; α' is the phase shift between the secondary windings of the phase-shift transformer and the phase voltage of the AFE; L_{AFE} is the AFE input inductance; R_{load} is the load resistance; LPF is the lowpass filter; SPG is the switching pattern generator, which can generate the SHE/SHM switching pattern $\{S_{SHE/SHM}\}$ based on θ, M, and α'. This experiment did not analyze the synthesis of the current and voltage control system. Controllers were synthesized using cascade control. To provide the stability and accuracy of a closed-loop system, it was necessary to consistently monitor that the values θ, M, and α' were constant during the operation of the system since the output accuracy of the SHE/SHM switching pattern $\{S_{SHE/SHM}\}$ through a switching pattern generator (SPG) can only be ensured this way. Only accurate SHE/SHM waveforms can ensure that the output results meet the system requirements. Therefore, an LPF was used to filter noise from the circuit, and the parameters of the PI controllers for the DC link voltage and current were carefully designed. Figure 7 shows the oscillograms of the instant AFE voltage values at a modulation index of 1.05. All oscillograms complied with the precalculated switching patterns.

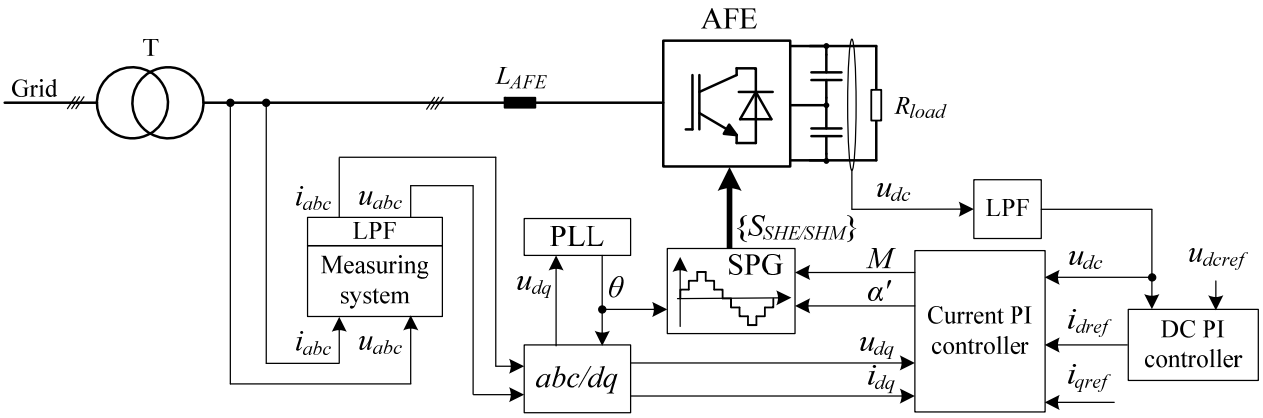

Figure 6. Circuit diagram of the AFE closed-loop control system.

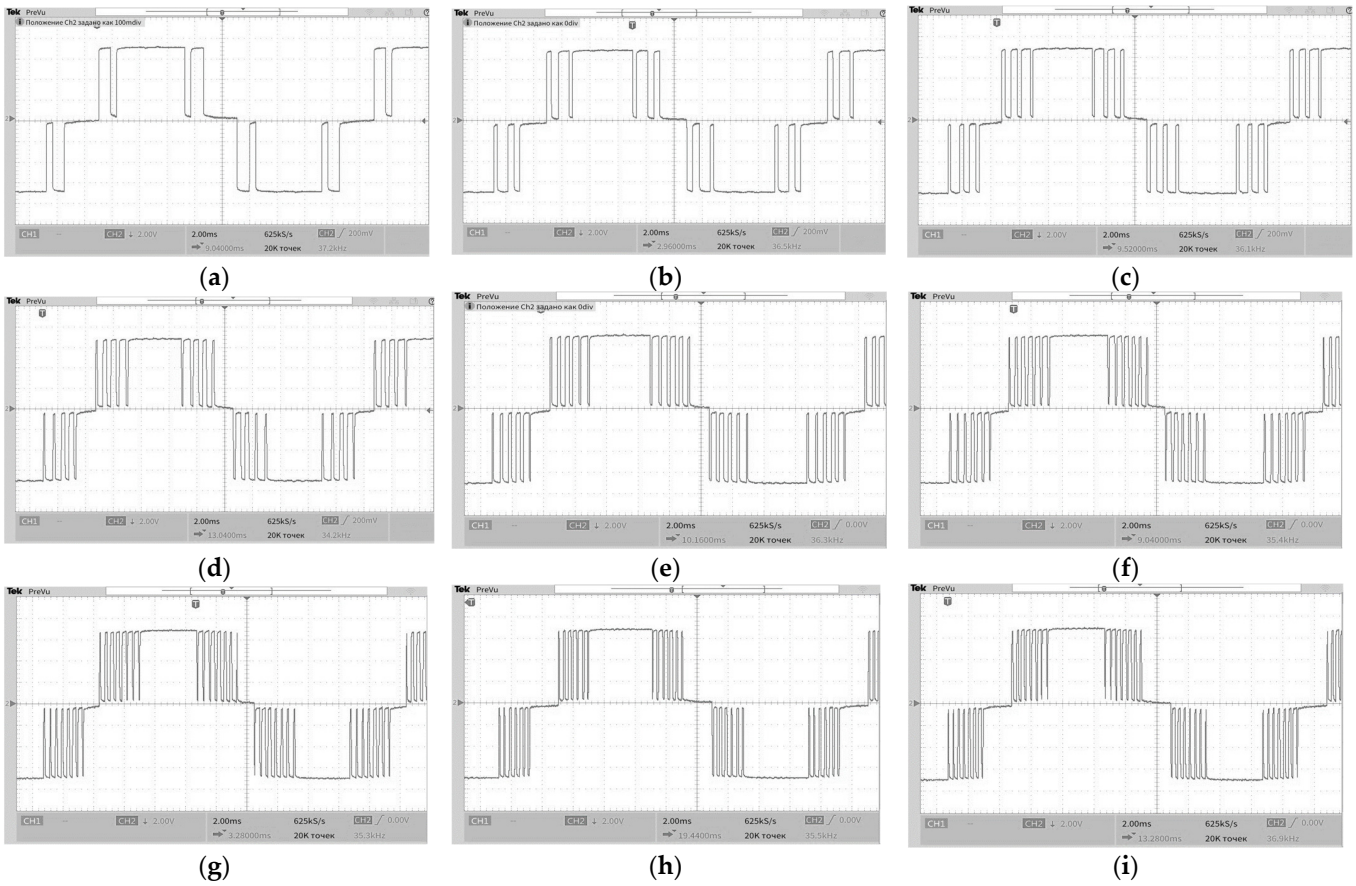

Figure 7. PPWM waveforms of the AFE converter: (**a**) SHE3; (**b**) SHE5; (**c**) SHE7; (**d**) SHE9; (**e**) SHE11; (**f**) SHE13; (**g**) SHE15; (**h**) SHM13; (**i**) SHM15.

4. Experimental Research Analysis

The impact of a three-level AFE featuring PPWM with SHE on current and voltage THD was studied at various ratios of AFE power S_{conv} and grid power S_{grid}. The range of S_{grid}/S_{conv} was selected between 30 and 230, accounting only for active inductive reactance. The current and voltage THD numbers were calculated up to the 50th and 100th harmonics for three different consumed AFE current values: $I = I_{rated}$, $I = 1.5\ I_{rated}$, and $I = 2\ I_{rated}$. All of the obtained dependencies for SHE3, SHE5, SHE7, SHE9, SHE11, SHE13, SHE15, SHM13, and SHM15 were rendered as graphs and are shown in Figures 8–10. Analysis of the results led to the following findings.

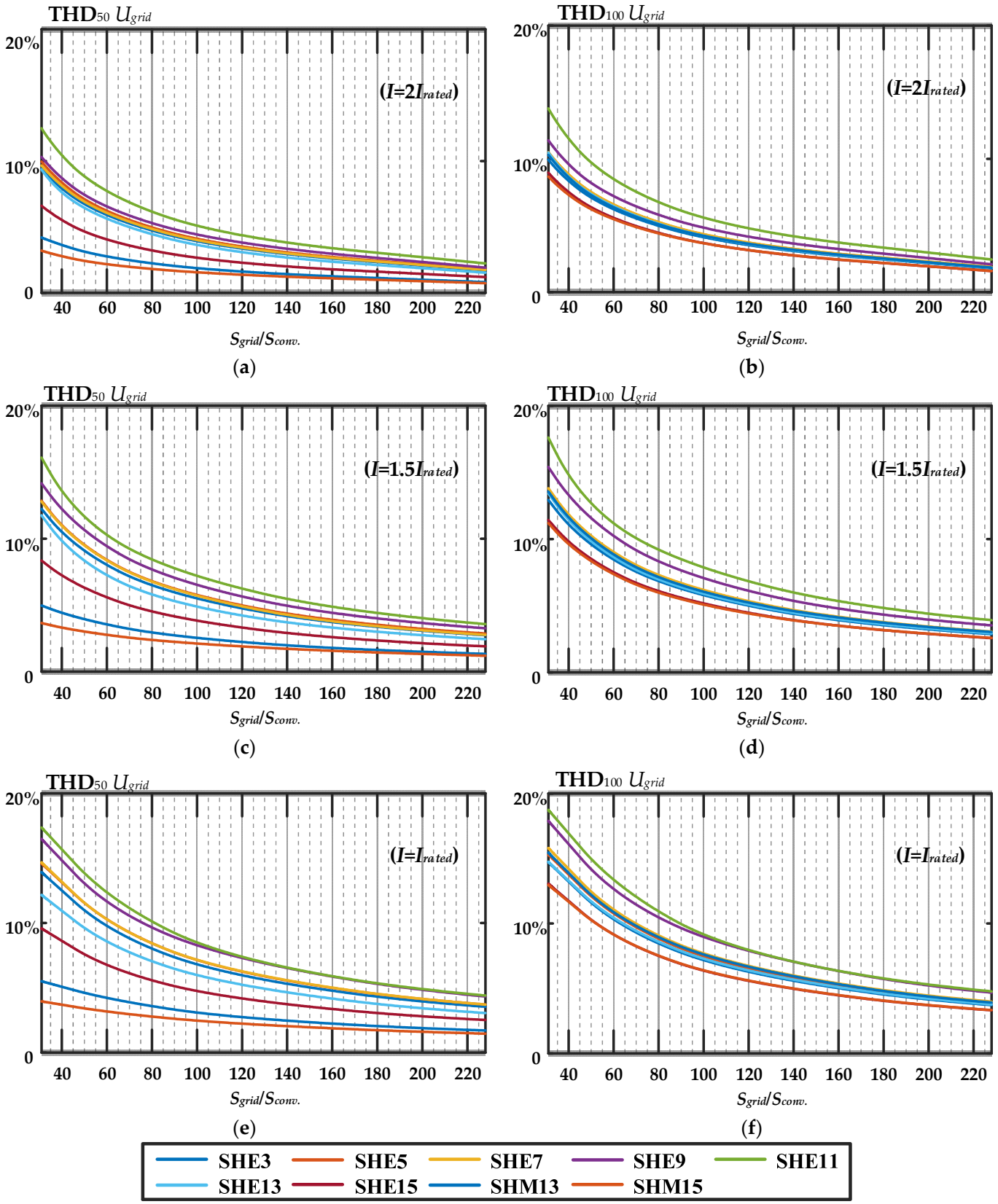

Figure 8. THD comparisons of U_{grid} between the harmonics up to the 50th order (**a**–**c**) and up to the 100th order (**d**–**f**).

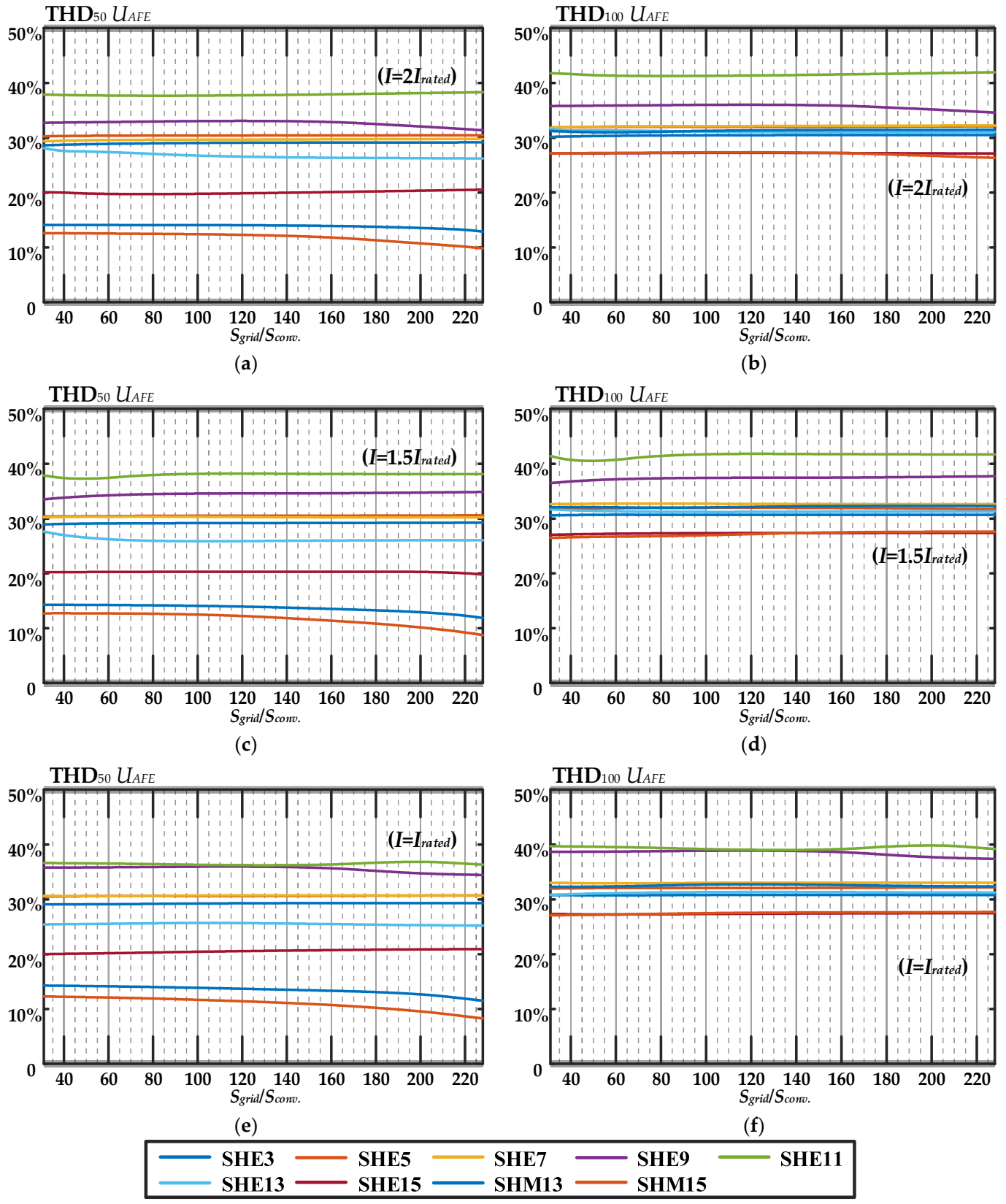

Figure 9. THD comparisons of U_{AFE} between the harmonics up to the 50th order (**a**–**c**) and up to the 100th order (**d**–**f**).

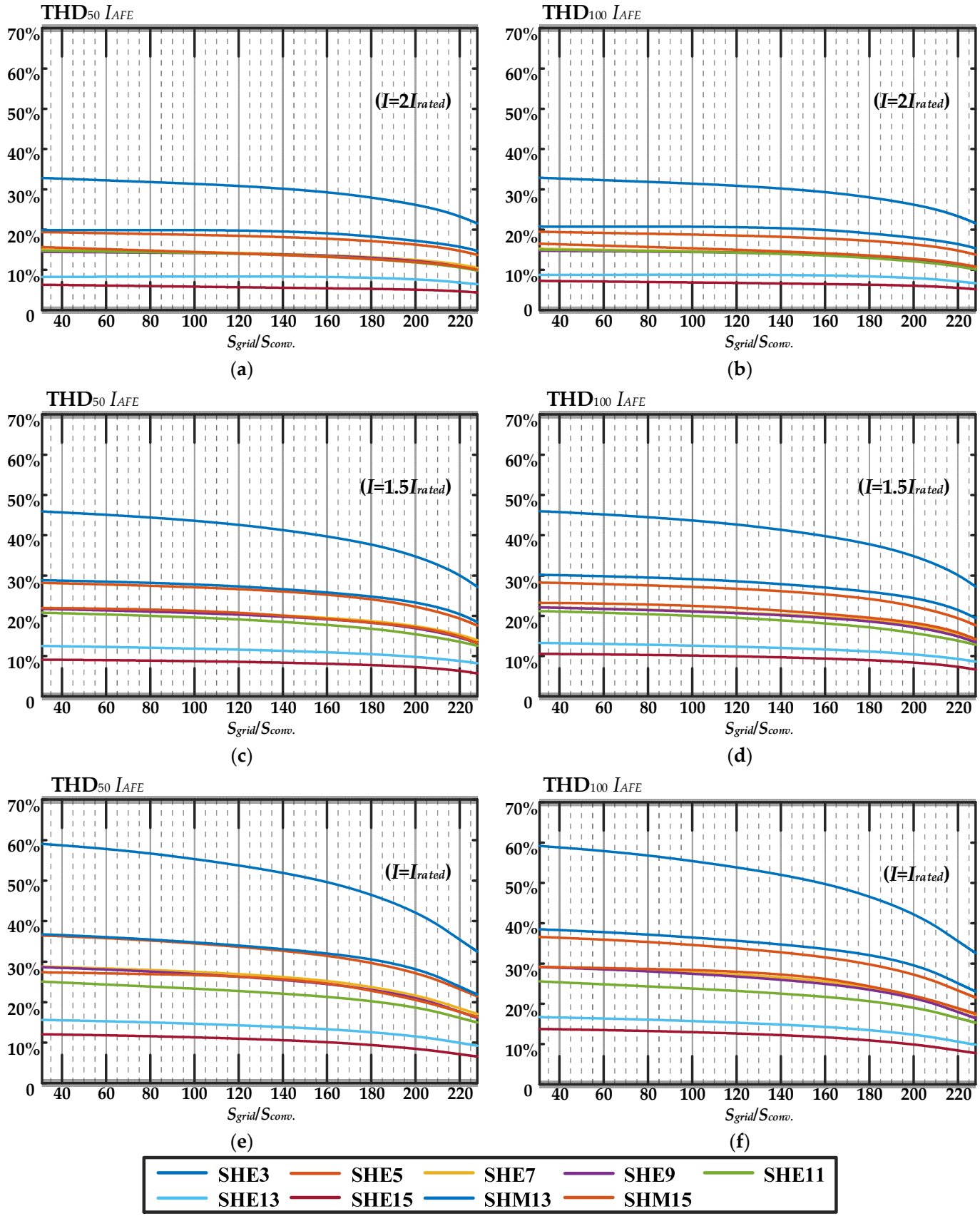

Figure 10. THD comparisons of I_{AFE} between the harmonics up to the 50th order (**a**–**c**) and up to the 100th order (**d**–**f**).

Figure 8 shows that the THD of grid voltage U_{grid} had the greatest distortion at $I = I_{rated}$ for both THD_{50} U_{grid} and THD_{100} U_{grid}. This can be explained by the reduction in the AFE modulation coefficients due to the reduction in the consumed current, which led to deterioration of the AFE voltage signal spectrum. As the consumed current increased from $I = I_{rated}$ to $I = 2$ I_{rated}, there was a downward trend for THD_{50} U_{grid} and THD_{100} U_{grid}. As expected, as the S_{grid}/S_{conv} ratio increased, THD_{50} U_{grid} and THD_{100} U_{grid} gradually decreased. Note that the rate of this downward trend varied across different S_{grid}/S_{conv} ranges, i.e., THD_{50} U_{grid} and THD_{100} U_{grid} decreased several times when S_{grid}/S_{conv} was between 30 and 120, while the reduction was less noticeable when S_{grid}/S_{conv} was between 120 and 230. If we compare THD_{50} U_{grid} and THD_{100} U_{grid}, we can see significant differences for all dependencies within the S_{grid}/S_{conv} range from 30 to 120, especially for SHM13 and SHM15. Furthermore, we can see that THD_{50} U_{grid} was significantly lower than THD_{100} U_{grid} (5–7 times lower in some cases). This was because the eliminated or mitigated harmonics were located in the PPWM spectrum below the 50th harmonic component. More importantly, if we follow THD_{100} U_{grid}, it approaches the same value in all calculated dependencies.

Figure 9 shows that the AFE voltage for both THD_{50} U_{AFE} and THD_{100} U_{AFE} did not change significantly when the current increased from $I = I_{rated}$ to $I = 2I_{rated}$ or when S_{grid}/S_{conv} changed. This is because the AFE voltage mainly depends on the PPWM algorithm and reliable control system operation. If we compare THD_{50} U_{AFE} and THD_{100} U_{AFE}, significant differences for SHM13 and SHM15 are observed. At the same time, the values of THD_{50} U_{AFE} differed for each of the calculated patterns. Thus, the positive impact of the increasing AFE switching rate on voltage quality is apparent. However, if we analyze THD_{100} U_{AFE}, the differences are not as significant, and sometimes there are no differences.

Figure 10 shows the current consumed by the AFE, I_{AFE}. The THD of the AFE current, I_{AFE}, had the greatest distortion, with $I = I_{rated}$ for both THD_{50} I_{AFE} and THD_{100} I_{AFE}. This can be explained by the reduction in the AFE modulation coefficients due to the reduction in the consumed current, which led to deterioration of the AFE voltage signal spectrum. As the consumed current increased from $I = I_{rated}$ to $I = 2$ I_{rated}, there was a downward trend for THD_{50} I_{AFE} and THD_{100} I_{AFE}. It should be noted that in all experiments, THD_{50} I_{AFE} and THD_{100} I_{AFE} had the same or virtually the same values. This is because within the spectrum of the AFE current, I_{AFE}, harmonics up to the 50th order had some impact, while the rest were mitigated by the inductive reactance of the grid. It should be noted that as the S_{grid}/S_{conv} ratio increased, THD_{50} I_{AFE} and THD_{100} I_{AFE} gradually decreased. The reduction rate was insignificant, and it differed notably from the grid voltage, as illustrated in Figure 8.

5. Conclusions

This article provides a comparative analysis of current and voltage THD in a circuit featuring a three-phase, three-level AFE with various switching patterns of PPWM and grid power. The experiments were conducted in a power conversion equipment laboratory. The results of the current and voltage THD comparison were calculated up to the 50th and 100th harmonics against the frequency of PPWM, with SHE ranging between 150 Hz and 750 Hz and the grid and the AFE power ratio between 30 and 230 under three different AFE-consumed currents.

This study demonstrates, for the first time, how the grid and AFE power ratio with different PPWM patterns can influence current and voltage THD. We observed that THD_{100} grid voltage approached the same value with all of the calculated PPWM patterns. Moreover, it was demonstrated that, as the PPWM switching frequency increased, the THD_{50} of the AFE voltage decreased significantly, but the THD_{100} analysis showed that the differences were not greatly significant and were sometimes absent. When high-power AFE rectifiers were used, it was reasonable to calculate THD to the 100th harmonic. This allows for a more accurate assessment of the AFE's electromagnetic compatibility compliance with the grid.

The research results suggest that it is necessary to review the existing calculation methods for current and voltage THD using modern electric power quality standards. In addition, the results also provide a reference point for researchers and engineers to consider the electromagnetic compatibility (EMC) of nonlinear consumers in the design of similar circuits.

Author Contributions: Conceptualization, A.S.M.; methodology, A.A.N. and A.S.M.; software, T.J. and A.S.M.; validation, A.A.N.; formal analysis, T.J.; investigation, T.J. and A.S.M.; resources, A.A.N. and A.S.M.; data curation, A.A.N.; writing—original draft preparation, A.S.M.; writing—review and editing, A.A.N. and T.J.; visualization, T.J.; supervision, A.S.M.; project administration, A.S.M. All authors have read and agreed to the published version of the manuscript.

Funding: This study was financially supported by the Moscow Polytechnic University (Pyotr Kapitsa grant).

Institutional Review Board Statement: Not applicable.

Informed Consent Statement: Not applicable.

Data Availability Statement: Not applicable.

Conflicts of Interest: The authors declare no conflict of interest.

Nomenclature

THD	Total harmonic distortion
AFE	Active front-end
PPWM	Preprogrammed pulse width modulation
NPC	Neutral-point-clamped
DC	Direct current
SHE	Selective harmonic elimination
SHE3	5th and 7th harmonic elimination
SHE5	5th, 7th, 11th, and 13th harmonic elimination
SHE7	5th, 7th, 11th, 13th, 17th, and 19th harmonic elimination
SHE9	5th, 7th, 11th, 13th, 17th, 19th, 23rd, and 25th harmonic elimination
SHE11	5th, 7th, 11th, 13th, 17th, 19th, 23rd, 25th, 29th, and 31st harmonic elimination
SHE13	5th, 7th, 11th, 13th, 17th, 19th, 23rd, 25th, 29th, 31st, 35th, and 37th harmonic elimination
SHE15	5th, 7th, 11th, 13th, 17th, 19th, 23rd, 25th, 29th, 31st, 35th, 37th, 41st, and 43rd harmonic elimination
SHM	Selective harmonic mitigation
SHM13	5th, 7th, 11th, 13th, 17th, 19th, 23rd, 25th, 29th, 31st, 35th, 37th, 41st, 43rd, 47th, and 49th harmonic mitigation
SHM15	5th, 7th, 11th, 13th, 17th, 19th, 23rd, 25th, 29th, 31st, 35th, 37th, 41st, 43rd, 47th, and 49th harmonic mitigation
VOC	Voltage-oriented control
PLL	Phase-locked loop
LPF	Low-pass filter
SPG	Switching pattern generator
CPLD	Complex programmable logic device
FPGA	Field-programmable gate array
DSP	Digital signal processor
T	Transformer
IGBT	Insulated-gate bipolar transistor
MIPS	Million instructions per second
S_{conv}	Converter power
S_{grid}	Grid power
I_{rated}	Rated AFE-consumed current
U_{grid}	Phase-to-phase grid voltage
U_{AFE}	Phase-to-phase AFE voltage

References

1. Leon, J.I.; Vazquez, S.; Franquelo, L.G. Multilevel converters: Control and modulation techniques for their operation and industrial applications. *Proc. IEEE* **2017**, *105*, 2066–2081. [CrossRef]
2. Abu-Rub, H.; Bayhan, S.; Moinoddin, S.; Malinowski, M.; Guzinski, J. Medium-Voltage Drives: Challenges and existing technology. *IEEE Power Electron. Mag.* **2016**, *3*, 29–41. [CrossRef]
3. Cheng, J.; Xu, T.; Chen, D.; Chen, G. Dynamic and steady state response analysis of selective harmonic elimination in high power inverters. *IEEE Access* **2021**, *9*, 75588–75598. [CrossRef]
4. Hoevenaars, A.; Farbis, M.; McGraw, M. Active harmonic mitigation: What the manufacturers don't tell you. *IEEE Ind. Appl. Mag.* **2020**, *62*, 41–51. [CrossRef]
5. Chen, J.; Shen, Y.; Chen, J.; Bai, H.; Gong, C.; Wang, F. Evaluation on the Autoconfigured Multipulse AC/DC Rectifiers and Their Application in More Electric Aircrafts. *IEEE Trans. Transp. Electrif.* **2020**, *6*, 1721–1739. [CrossRef]
6. Patil, S.D.; Kadu, A.; Dhabe, P. Improved Control Strategy for Harmonic Mitigation in Multilevel Inverter. In Proceedings of the 5th International Conference on Intelligent Computing and Control Systems, Madurai, India, 6–8 May 2021; pp. 727–732.
7. Steczek, M.; Chudzik, P.; Szeląg, A. Combination of SHE- and SHM-PWM techniques for VSI DC-link current harmonics control in railway applications. *IEEE Trans. Ind. Electron.* **2017**, *64*, 7666–7678. [CrossRef]
8. Nikolaev, A.A.; Gilemov, I.G.; Denisevich, A.S. Analysis of Influence of Frequency Converters with Active Rectifiers on the Power Quality in Internal Power Supply Systems of Industrial Enterprises. In Proceedings of the International Conference on Industrial Engineering, Applications and Manufacturing, Moscow, Russia, 1–4 May 2018.
9. Portillo, R.; Sharifzadeh, M.; Vahedi, H.; Franquelo, L.G.; Al-Haddad, K. Improved Hybrid SHM-SHE Modulation Technique 865 for Four-Leg Three-Level NPC Inverters. In Proceedings of the IECON 2015-41st Annual Conference of the IEEE Industrial 866 Electronics Society, Yokohama, Japan, 9–12 November 2015.
10. Campos-Gaona, D.; Peña-Alzola, R.; Monroy-Morales, J.L.; Ordonez, M.; Anaya-Lara, O.; Leithead, W.E. Fast selective harmonic mitigation in multifunctional inverters using internal model controllers and synchronous reference frames. *IEEE Trans. Ind. Electron.* **2017**, *64*, 6338–6349. [CrossRef]
11. Su, N.; Huang, W.; Zheng, S. Closed-loop dynamic control for dual-stator winding induction generator at low carrier ratio with selective harmonic elimination pulsewidth modulation. *IEEE Trans. Ind. Electron.* **2020**, *68*, 4737–4747. [CrossRef]
12. Sharifzadeh, M.; Vahedi, H.; Sheikholeslami, A.; Labbé, P.; Al-Haddad, K. Hybrid SHM–SHE modulation technique for a four-leg NPC inverter with DC capacitor self-voltage balancing. *IEEE Trans. Ind. Electron.* **2015**, *62*, 4890–4899. [CrossRef]
13. Janabi, A.; Wang, B.; Czarkowski, D. Generalized Chudnovsky algorithm for real-time PWM selective harmonic elimination/modulation: Two-Level VSI example. *IEEE Trans. Power Electron.* **2020**, *35*, 5437–5446. [CrossRef]
14. Marquez Alcaide, A.; Leon, J.I.; Laguna, M.; Gonzalez-Rodriguez, F.; Portillo, R.; Zafra-Ratia, E.; Vazquez, S.; Franquelo, L.G.; Bayhan, S.; Abu-Rub, H. Real-Time Selective Harmonic Mitigation Technique for Power Converters Based on the Exchange Market Algorithm. *Energies* **2020**, *13*, 1659. [CrossRef]
15. Moeini, A.; Zhao, H.; Wang, S. A current-reference-based selective harmonic current mitigation PWM technique to improve the performance of cascaded H-bridge multilevel active rectifiers. *IEEE Trans. Ind. Electron.* **2018**, *65*, 727–737. [CrossRef]
16. Nikolaev, A.A.; Gilemov, I.G.; Bulanov, M.V.; Kosmatov, V.I. Providing Electromagnetic Compatibility of High-Power Frequency Converters with Active Rectifiers at Internal Power Supply System of Cherepovets Steel Mill. In Proceedings of the International Scientific Technical Conference Alternating Current Electric Drives, Ekaterinburg, Russia, 1–8 May 2021.
17. de Carvalho Alves, M.D.; e Silva Aquino, R.N.A.L. Digital implementation of SHE-PWM modulation on FPGA for a multilevel inverter. In Proceedings of the Simposio Brasileiro de Sistemas Eletricos (SBSE), Niteroi, Brazil, 1–6 May 2018. [CrossRef]
18. Janabi, A.; Wang, B. Real-Time Implementation of Selective Harmonic Elimination with Seamless Dynamic Performance. In Proceedings of the IEEE Energy Conversion Congress and Exposition, Portland, OR, USA, 23–27 September 2018; pp. 3362–3366.
19. Aguilera, R.P.; Acuña, P.; Lezana, P.; Konstantinou, G.; Wu, B.; Bernet, S.; Agelidis, V.G. Selective harmonic elimination model predictive control for multilevel power converters. *IEEE Trans. Power Electron.* **2017**, *32*, 2416–2426. [CrossRef]
20. Sharifzadeh, M.; Vahedi, H.; Portillo, R.; Franquelo, L.G.; Al-Haddad, K. Selective harmonic mitigation based self-elimination of triplen harmonics for single-phase five-level inverters. *IEEE Trans. Power Electron.* **2019**, *34*, 86–96. [CrossRef]
21. González, F.J.; Marquez, A.; Leon, J.I.; Vazquez, S.; Franquelo, L.G.; Yin, J. Flexible Harmonic Control for Three-Level Selective Harmonic Modulation Using the Exchange Market Algorithm. In Proceedings of the IECON 2018—44th Annual Conference of the IEEE Industrial Electronics Society, Washington, DC, USA, 21–23 October 2018; pp. 5297–5302.
22. Semedyarov, A.; Ruderman, A. Selective Harmonic Mitigation by Time Domain Constrained Optimization. In Proceedings of the 9th IEEE International Symposium on Power Electronics for Distributed Generation Systems, Charlotte, CA, USA, 1–6 June 2018.
23. Buccella, C.; Cimoroni, M.G.; Cecati, C. Simple SHE Formulation for Five-Level Cascaded H-Bridge Inverters. In Proceedings of the IEEE 15th International Conference on Compatibility, Power Electronics and Power Engineering, Florence, Italy, 1–6 July 2021.
24. Buccella, C.; Cimoroni, M.G.; Cecati, C. Selective Harmonic Elimination Modulation for HVDC Modular Multilevel Converter. In Proceedings of the AEIT HVDC International Conference, Genoa, Italy, 1–6 May 2021.
25. Khattak, F.A.; Rehman, H.U. Improved Selective Harmonics Elimination Strategy for Multilevel Inverters with Optimal DC Values. In Proceedings of the International Conference on Emerging Power Technologies, Topi, Pakistan, 1–6 April 2021.
26. Islam, J.; Meraj, S.T.; Masaoud, A.; Mahmud, M.A.; Nazir, A.; Kabir, M.A.; Hossain, M.M.; Mumtaz, F. Opposition-based quantum bat algorithm to eliminate lower-order harmonics of multilevel inverters. *IEEE Access* **2021**, *9*, 103610–103626. [CrossRef]

27. Sadoughi, M.; Zakerian, A.; Pourdadashnia, A.; Farhadi-Kangarlu, M. Selective Harmonic Elimination PWM for Cascaded H-bridge Multilevel Inverter with Wide Output Voltage Range Using PSO Algorithm. In Proceedings of the IEEE Texas Power and Energy Conference, College Station, TX, USA, 1–6 February 2021.
28. Aggrawal, H.; Leon, J.I.; Franquelo, L.G.; Kouro, S.; Garg, P.; Rodriguez, J. Innovative Computational Approach to Harmonic Mitigation for Seven-Level Cascaded H-Bridge Inverters. In Proceedings of the IECON 2011—37th Annual Conference of the IEEE Industrial Electronics Society, Melbourne, Australia, 7–10 November 2021; pp. 4424–4432.
29. Ahmad, S.; Iqbal, A.; Ali, M.; Rahman, K.; Ahmed, A.S. A fast convergent homotopy perturbation method for solving selective harmonics elimination PWM problem in multi level inverter. *IEEE Access* **2021**, *9*, 113040–113051. [CrossRef]
30. Gabour, N.E.H.; Habbi, F.; Bounekhla, M.; Boudissa, E.G. Enhanced Harmonic Elimination Using Genetic Algorithm Optimization in Multilevel Inverters. In Proceedings of the 18th International Multi-Conference on Systems, Signals & Devices, Monastir, Tunisia, 22–25 March 2021; pp. 323–329.
31. Padmanaban, S.; Dhanamjayulu, C.; Khan, B. Artificial neural network and Newton Raphson (ANN-NR) algorithm based selective harmonic elimination in cascaded multilevel inverter for PV applications. *IEEE Access* **2021**, *9*, 75058–75070. [CrossRef]
32. Memon, M.A.; Siddique, M.D.; Saad, M.; Mubin, M. Asynchronous particle swarm optimization-genetic algorithm (APSO-GA) based selective harmonic elimination in a cascaded H-bridge multilevel inverter. *IEEE Trans. Ind. Electron.* **2022**, *69*, 1477–1487. [CrossRef]
33. Jiang, Y.; Li, X.; Qin, C.; Xing, X.; Chen, Z. Improved particle swarm optimization based selective harmonic elimination and neutral point balance control for three-level inverter in low-voltage ride-through operation. *IEEE Trans. Ind. Inform.* **2022**, *18*, 642–652. [CrossRef]